Sustainable Materials and Technologies 43 (2025) e01275

Contents lists available at ScienceDirect

Sustainable Materials and Technologies

journal homepage: www.elsevier.com/locate/susmat

An experimental demonstration on the recyclability of hybrid magnetite-humic acid nanoparticles

Gabriele Bona [a], Lorenzo Viganò [a], Matteo Cantoni [b], Roberto Mantovan [c], Barbara Di Credico [a], Silvia Mostoni [a], Roberto Scotti [a,d], Roberto Nisticò [a,*]

[a] University of Milano-Bicocca, Department of Materials Science, U5, INSTM, Via R. Cozzi 55, 20125 Milano, Italy
[b] Politecnico di Milano, Department of Physics, Via G. Colombo 81, 20133 Milano, Italy
[c] CNR-IMM, Unit of Agrate Brianza, Via. C. Olivetti 2, 20864 Agrate Brianza (MB), Italy
[d] Institute for Photonics and Nanotechnologies-CNR, Via alla Cascata 56/C, 38123 Povo (TN), Italy

ARTICLE INFO

Keywords:
Humic acid
Hybrid magnetite
Iron oxides
Magnetic materials
Photocatalysis
Recyclability

ABSTRACT

In this study, hybrid magnet-sensitive nanoparticles made by magnetite and humic acid are primarily obtained following a co-precipitation route. Subsequently, such hybrid systems are fully recycled following a two-step process, namely: (i) calcination under air (oxidizing) atmosphere, and (ii) acid digestion to obtain an Fe(III) aqueous solution. After neutralization, hybrid magnet-sensitive nanoparticles are re-synthesized following a properly modified synthetic route analogous to the previous one. Both hybrid nanoparticles are characterized by means of different morphological, structural, physicochemical, and magnetic techniques. Additionally, these magnet-sensitive hybrids are tested in the photocatalytic abatement of paracetamol from model wastewater, investigating a photo-Fenton degradation route. Experimental results evidence a superimposable degradation profiles of both hybrid nanoparticles, with an almost complete degradation of paracetamol after 120 min of UV irradiation (with 96–98 % of abatement). These results clearly demonstrate that the recycling route here proposed is an effective approach for the virtuous recycling of these hybrid nanoparticles, and the photocatalytic tests, although preliminary, encourage on the possibility of using these magnetic systems as substrates for the sustainable abatement of recalcitrant emerging micro-contaminants in wastewater treatments.

1. Introduction

In today's world, the continuous anthropogenic impact on our planet is creating a dramatic depletion of the available resources, and a serious alarm regarding the clean water scarcity [1,2], with ca. 3.6 billion people (i.e., almost half of the human population) living in countries that suffer water scarcity [3]. Considering these aspects, it clearly emerges the importance of exploring integrated water reuse and water treatment processes seeking for a transition toward a more circular water management [4]. Among the different inorganic nanomaterials exploitable in the photocatalytic remediation of contaminated wastewater, the most promising substrates are metallic systems (e.g., AgNPs, ZVI), and metal oxides, such as titania (TiO_2), zinc oxide (ZnO), and iron oxides nanoparticles, with TiO_2 being the most common photocatalyst due to its high photocatalytic activity, reasonable cost, photo-, chemical and biological stability [5–7].

In this context, magnetic iron oxide nanomaterials have attracted growing interest in water treatments as low cost and environmental-friendly substrates, easily recoverable (simply by applying an external magnetic field), and showing great performances as heterogeneous catalysts in (photo)-Fenton processes [8–15]. The catalytic mechanism involving iron oxides can be twofold: (i) a heterogeneous action involving the electron/hole separation and formation of hydroxyl radicals [16], and (ii) a homogeneous action involving the leaching of iron ions from the solid surface [17]. Based on our personal expertise, it has been fully demonstrated that magnetic iron oxides (i.e., magnetite) nanoparticles partially covered with humic-like substances [18–20] are very promising hybrid materials for the photocatalytic abatement of different emerging contaminants from wastewater media, such as Carbamazepine [21], Caffeine [4,22], Diclofenac [13], Flumequine [21], Ibuprofen [21], Sulfamethoxazole [21], and many others. However, this might not be enough. In fact, despite the numerous public demonstrations in support of climate and ecological activism have risen up the attention on water emergency, the recent energetic crisis has also

* Corresponding author.
E-mail address: roberto.nistico@unimib.it (R. Nisticò).

https://doi.org/10.1016/j.susmat.2025.e01275
Received 31 October 2024; Received in revised form 9 December 2024; Accepted 25 January 2025
Available online 27 January 2025

pointed out the importance of developing technological solutions based on renewable energy and materials with closed life cycles. Hence, the reuse of materials is becoming a key point to save minerals and raw materials, reducing the production of waste and pollution degree of the environment. Translating this key point to the direct use of hybrid nanosystems made by magnetite and humic acids (HA) for the environmental remediation of contaminated wastewater, it becomes legitimate to ask whether this approach is a sustainable technological solution or not, and in particular which is the fate of the hybrid magnetite-HA nanoparticles once their use has ended. Is it possible to fully recycle end-of-life hybrid magnetite-HA nanoparticles, reaching a closed life cycle?

This last aspect has been poorly investigated in the state-of-the-art literature. In fact, in the study by Nyabadza et al. [23], it has been reported that even if nanomaterials have shown great potential in the treatment of contaminated wastewater, a recycling or disposal plan after their use is a mandatory point, in order to ensure a full sustainability. In this context, the separation of the nanomaterials from water is a crucial step that demands careful attention. Multiple approaches have been developed for recycling or disposing nanomaterials, with magnetic separation and flocculation being the most promising ones [23]. However, in most cases, the preferred disposal strategy still remains the immobilization of regenerated nanomaterials into composite matrices or their direct incineration (see [23], and references therein). Interestingly, in the study by Gautam et al. [24], hybrid magnetite nanoparticles functionalized with HA were used as adsorbents for the removal of dye molecules from water. In their studies, the authors reported the possibility of desorbing the adsorbate molecules in presence of 0.1 M HCl and recycling the magnetite nanoparticles by performing five adsorption/desorption processes. Results indicate a progressive reduction of the magnetic nanomaterials' sorption capacity and efficiency with the number of their reuses.

On the contrary, the present study aims to evaluate the possibility to fully recycle end-of-life hybrid magnetite-HA nanoparticles, by resynthesizing newly hybrid nanoparticles starting from the exhausted ones. This last aspect is a poorly investigated topic, since in most of the literature, the synthesis of magnetite nanoparticles involves mineral waste (e.g., iron ore tailings) [25], and not previously prepared nanomaterials. Here, hybrid magnetite-HA nanoparticles were synthesized by means of a well-established co-precipitation route from exhausted hybrid magnetic nanoparticles [21,26,27]. First, such nanoparticles were calcined under air (oxidizing) atmosphere in order to both burn away the organic fraction deriving from the residual HA, and convert the inorganic fraction (i.e., partially-reduced magnetite Fe_3O_4) into the fully oxidized hematite α-Fe_2O_3. Lastly, with the purpose of isolating ferric ions into a more usable form, hematite has been acid digested, obtaining a Fe(III) aqueous solution [28]. After neutralization, hybrid magnetite-HA nanoparticles were resynthesized following a co-precipitation route analogous to the previous one, thus obtaining recycled hybrid magnetite-HA (RHM) nanoparticles. The entire procedure is reported in Fig. 1.

Morphological, structural and physicochemical properties of both HM and RHM were monitored by means of multiple techniques, such as scanning electron microscopy (SEM), X-ray powder diffraction (XRD), thermal gravimetric analysis (TGA), Fourier transform infrared (FTIR) spectroscopy, transmission Mössbauer (TMS) spectroscopy, and vibrating sample magnetometry (VSM). Lastly, to evaluate the efficiency of both HM and RHM in terms of photocatalytic abatement against paracetamol as target pollutant, preliminary photo-Fenton degradation experiments were carried out. In particular, paracetamol (a non-steroidal anti-inflammatory drug) is an emerging pollutant among the sixteen substances detected in surface, drinking, and groundwater, with global average concentrations ranging between ca. 0.030 to 0.920 μg L^{-1} (i.e., low concentration, and relatively difficult to be removed), and being highly biologically active [29].

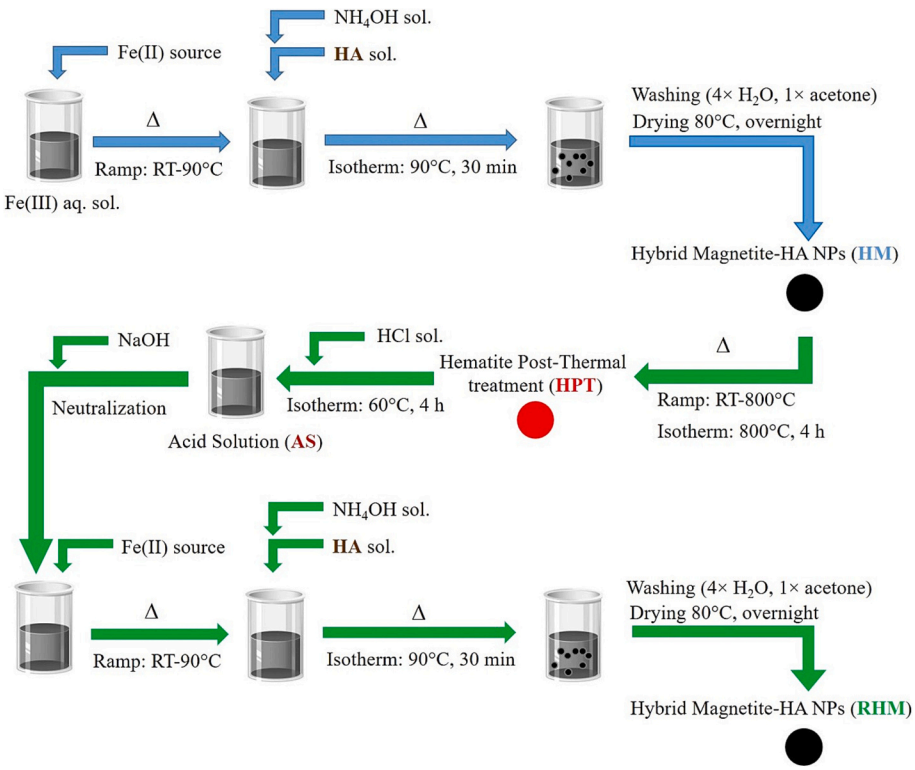

Fig. 1. Scheme of the direct synthesis of HM, and the recycling route proposed for the synthesis of RHM from HM.

2. Experimental section

2.1. Chemicals

Reactants: Iron(II) sulfate heptahydrate ($FeSO_4{\cdot}7H_2O$, 98 %, CAS 7782-63-0, Thermo Scientific), iron(III) chloride hexahydrate ($FeCl_3{\cdot}6H_2O$, CAS 10025–77-1, VWR Chemicals), paracetamol ($C_8H_9NO_2$, 78 %, CAS 103–90-2, Thermo Scientific), and humic acid sodium salt (HA, tech. 50–60 % as humic acid, CAS 68131–04-4, Thermo Scientific) were used as received. Potassium bromide (KBr, 99 + %, FTIR grade, CAS 7758-02-3, Aldrich) was heated at *approx*. 80 °C prior to use to maintain it dry. Solutions and solvents: Ammonia solution (25 %, ISO. Reag, Ph. Eur., CAS 1336-21-6, Supelco), 6 M HCl solution prepared by diluting hydrochloric acid (HCl, puriss., p.a., ACS reagent. ISO, reag. Ph. Eur., fuming ≥37 %, CAS 7647-01-0, Sigma-Aldrich) in deionized water, 6 M NaOH solution prepared by dissolving sodium hydroxide pellets (NaOH, puriss., p.a., ACS reagent, ≥ 98 %, CAS 1310-73-2, Aldrich) in deionized water, hydrogen peroxide solution (H_2O_2, 35 wt%, CAS 7722-84-1, Alfa Aesar), acetone (CH_3COCH_3, CAS 67–64-1, Sigma-Aldrich). Furthermore, deionized water was used during washing procedures. Milli-Q water with a resistivity of 18.2 MΩ cm was used. All chemicals were used without further purification.

2.2. Synthesis of hybrid magnetite via co-precipitation mechanism

Hybrid magnetite nanoparticles are prepared following a modified procedure taken from the literature [21,26,27]. In detail, iron(II) sulfate heptahydrate (4.17 g) and iron(III) chloride hexahydrate (6.17 g) were introduced into a beaker (with Fe(III)/Fe(II) molar ratio of ca. 1.5), and dissolved in 100 mL of deionized water by means of magnetic stirring. The obtained solution was heated from RT to 90 °C. Once the target temperature was reached, two solutions were added simultaneously: (i) 25 % ammonia solution (10 mL), and (ii) previously prepared 2 wt% HA aqueous solution (50 mL). Immediately, hybrid magnetite nanoparticles precipitate in the alkaline medium, forming a dark-brown suspension. Such suspension was maintained under magnetic stirring at isothermal conditions (90 °C for 30 min), and then cooled down to RT. Hybrid magnetite nanoparticles were separated from the aqueous medium by performing a magnetic separation (applying a commercial neodymium magnet). Afterwards, hybrid magnetite nanoparticles were centrifuged at 4000 rpm for 30 min, washing with deionized water (four times) and acetone (one time), in order to remove the possible reaction by-products (i.e., residual ammonium salts). Purified suspension of hybrid magnetite nanoparticles was deposited over a glass Petri dish and oven dried under air atmosphere at 80 °C overnight. Lastly, dried hybrid magnetite nanoparticles were gently crumbled inside an agate mortar, and sample stored inside a closed glass vial (yield 89.7 %). The obtained sample was defined as HM (acronym of Hybrid Magnetite). Furthermore, for the sake of comparison, a bare magnetite (defined as M0) obtained following the previous procedure in absence of HA, has been taken as reference substrate.

2.3. Thermal treatment and acid digestion of hybrid magnetite

The controlled degradation of the hybrid magnetite nanoparticles was carried out by performing two subsequent treatments: a preliminary thermal treatment under oxidizing conditions, followed by an acid digestion. The thermal treatment was performed by depositing the HM sample (ca. 1.3 g) on an alumina vessel and introducing it inside a Carbolite CWF1200 muffle furnace (*Carbolite, Hope, UK*), operating under air (oxidizing) atmosphere. The applied thermal program was the following: (i) heating ramp from RT to 800 °C (heating rate: 10 °C min^{-1}), (ii) isothermal step at 800 °C for 4 h, and (iii) cooling step from 800 °C to 50 °C (cooling rate: 5 °C min^{-1}). Subsequently, the sample was allowed to cool down from 50 °C to RT naturally. At the end of the thermal treatment, the organic fraction of the HM sample (deriving from the HA fraction) was evolved as volatiles, whereas the inorganic fraction of the HM sample (deriving from the iron oxide fraction) was oxidized to hematite (the most thermodynamically stable form of iron(III) oxide). The hematite solid residue was defined as HPT (acronym of Hematite Post-Thermal treatment). The acid digestion was performed by introducing in a beaker a known amount of HPT (ca. 1.0 g), and dissolving the sample in 20 mL of 6 M HCl solution by means of magnetic stirring at 60 °C for 4 h. During this step, the hematite deriving from the previous thermal treatment (HPT sample) was fully solubilized as Fe(III) acid solution, defined as AS (acronym of Acid Solution).

2.4. Synthesis of recycled hybrid magnetite via co-precipitation mechanism

In order to balance the pH of the AS, it was mandatory prior to neutralize the acid environment. To do this, ca. 20 mL of 6 M NaOH solution were added dropwise very slowly to the solution at RT under vigorous magnetic stirring, in order to avoid the immediate precipitation of ferric hydroxide. Hence, the calculated concentration of Fe(III) in the neutralized AS is expected being 0.31 M. Therefore, recycled hybrid magnetite nanoparticles were prepared re-scaling the previously described procedure. In detail, iron(II) sulfate heptahydrate (2.25 g) were introduced into a beaker, and dissolved in 40 mL of neutralized AS (thus still maintaining the stoichiometric Fe(III)/Fe(II) molar ratio of ca. 1.5) by means of magnetic stirring. Deionized water (14 mL) were added to the medium, thus obtaining the final volume being equal to 54 mL. The obtained solution was heated from RT to 90 °C. Once the target temperature was reached, two solutions were added simultaneously: (i) 25 % ammonia solution (5.4 mL), and (ii) previously prepared 2 wt% HA aqueous solution (27 mL). Immediately, hybrid magnetite nanoparticles precipitate in the alkaline medium, forming a dark-brown suspension. Such suspension was maintained under magnetic stirring at isothermal conditions (90 °C for 30 min), and then cooled down to RT. Hybrid magnetite nanoparticles were separated from the aqueous medium by performing a magnetic separation (applying a commercial neodymium magnet). Afterwards, hybrid magnetite nanoparticles were centrifuged at 4000 rpm for 30 min, washing with deionized water (four times) and acetone (one time), in order to remove the possible reaction by-products (i.e., residual ammonium salts, sodium chloride). Purified suspension of hybrid magnetite nanoparticles was deposited over a glass Petri dish and oven dried under air atmosphere at 80 °C overnight. Lastly, dried hybrid magnetite nanoparticles were gently crumbled inside an agate mortar, and sample storage inside a closed glass vial (yield 65.5 %). The obtained sample was defined as RHM (acronym of Recycled Hybrid Magnetite).

2.5. Morphological, physicochemical, and magnetic characterizations

Scanning electron microscopy (SEM) micrographs were collected by means of a Zeiss Gemini 500 microscope equipped with a traditional electron detector and the Bruker Quantax detector for energy dispersive X-ray spectroscopy (EDS) microanalysis. Samples were deposited onto SEM stubs using a double-adhesive carbon tape for SEM-EDS analysis. Stabs were covered with a gold coating to avoid any charging effect by means of an Edwards S150B sputter coater.

X-ray powder diffraction (XRD) patterns were recorded by means of a Rigaku Miniflex 600. The acquisition was performed using a Cu source (40 kV, 15 mA), scanning in the 20–70°2θ range, with a step size of 0.02 degrees, angular velocity 5.0 degrees per minute. Instrumental PDXL-2 software was used for the sake of comparison with reference diffraction patterns from the ICDD database. The crystallite average size was estimated by means of the Scherrer equation (Eq. (1)):

$$\tau = \frac{K\lambda}{\beta cos\theta} \quad (1)$$

where τ is the average size of the crystalline domains (expressed in nm), K is the shape factor (typically 0.9), λ is the X-ray wavelength (0.154 nm for a Cu source), β is the line broadening at half the maximum intensity (FWHM) of the selected Bragg angle after subtracting the instrumental line broadening (expressed in radians), and θ is the Bragg angle (expressed in radians). Regarding the magnetite systems, the Bragg angle selected was the crystal reflection at ca. $2\theta = 35.4°$, corresponding to the Miller index (311).

Thermogravimetric analysis (TGA) thermograms were collected by using a Mettler Toledo TGA/DSC1 STARe system at a constant air flow (50 cm^3 min^{-1}). Measurements were performed on open alumina sample holder, with the following thermal program: heating ramp from 30 °C to 150 °C (heating rate: 10 °C min^{-1}), isothermal step at 150 °C for 10 min, heating ramp from 150 °C to 1000 °C (heating rate: 10 °C min^{-1}), isothermal step at 1000 °C for 5 min.

Fourier transform infrared (FTIR) spectra were recorded in transmission mode by means of a Jasco-4100 spectrophotometer, equipped with DTGS detector, applying the Blackman-Harris apodization function, and working with 128 scans at 4 cm^{-1} resolution in the 4000–400 cm^{-1} range. Samples were dispersed in dried KBr (1:100 wt. ratio), manually grinded inside an agate mortar, and hydraulic pressed to obtain homogeneous pellets.

2.6. Photocatalytic testing

Photocatalytic experiments were performed in a 0.5 L cylindrical Pyrex batch photoreactor equipped with an external cooling jacket, enveloped by aluminium foil, in presence of a 125 W medium-pressure Hg lamp (*Helios Italquartz, Italy*), with a maximum emission at about 365 nm, axially immersed within the photoreactor [30]. The temperature of the solution has been maintained at 25 ± 2 °C by the circulation system through a jacket surrounding the reactor. In the case of the heterogenous systems, the suspension has been kept in the dark for ca. 0.5 h to reach the adsorption-desorption equilibrium, before adding 180 μL of a H_2O_2 solution 35 wt% (final concentration 3.7 mM) and switching on the UV lamp. A magnetic stirrer was used to guarantee the homogeneity of the reaction mixture. The concentration of the magnetite-based nanomaterials was 100 mg L^{-1} (ca. 50 mg), whereas the initial paracetamol concentration was 30 mg L^{-1}. Control experiments were carried out in homogeneous conditions (i.e., in absence of the nanomaterials) to evaluate the photolysis (only UV irradiation) and the photostability of paracetamol in presence of H_2O_2 (UV/H_2O_2). Aliquots (4 mL) were taken at different time intervals (0, 15, 30, 60, 90, 120, and 150 min) to evaluate the progress of paracetamol degradation. For each aliquot, the presence of suspended magnetite has been removed by performing a magnetic separation (by using a commercially available neodymium disc magnet, diameter 42 mm, strength ca. 12 kg; *Supermagnete, Germany*) and the supernatant solution filtrated through a 0.22 μm hydrophilic PTFE syringe filter. All tests were performed in duplicate. The quantitative determination of the paracetamol was performed by means of a single beam Cary 60 UV/Vis spectrophotometer (*Agilent Technologies*) measuring with scam control medium in the 190–800 nm range (absorption maximum at 245 nm). The degradation efficiency (expressed as C/C_0) of paracetamol was calculated applying the following formula (Eq. (**2**)):

$$\frac{C}{C_0} = \frac{Abs^{t}_{245\ nm}}{Abs^{-30\ min}_{245\ nm}} \times 100 \quad (2)$$

where $Abs^{t}_{245\ nm}$ is the integral value of the absorption signal at 245 nm at a given time t, and $Abs^{-30\ min}_{245\ nm}$ is the integral value of the absorption signal at 245 nm at time − 30 min (i.e., in the dark). The absorption signal of Milli-Q water was taken as reference for the baseline correction.

3. Results and discussion

3.1. Evaluation of the recycling process: Morphological, structural, thermal, physicochemical, and magnetic characterization

Fig. 2 reports the morphological (SEM) and structural (XRD) characterization of magnetic nanomaterials coming from the recycling process, namely the reference bare magnetite (M0), both the freshly prepared HM and resynthesized RHM nanomaterials, as well the hematite phase deriving from the thermal treatment proposed in the HM-to-RHM recycling process (i.e., HPT). The morphological analysis of the reference bare magnetite (M0) reveals the formation of pseudo-spherical aggregates of nanoparticles with average diameter of ca. 80–100 nm (Fig. 2A'), whereas the XRD pattern of M0 shows the main relevant reflections at $2\theta = 30.1°$ (220), 35.4° (311), 43.1° (400), 53.4° (422), 57.0° (333), and 62.6° (440), which can be associated to the presence of the magnetite crystal phase (card number 01–074-0748, ICDD, Fig. 2A) [4,31]. No extra peaks are detected, confirming the purity of the sample. Interestingly, the freshly prepared HM nanomaterial after the co-precipitation route here proposed shows a similar morphology compared to the reference M0, with formation of pseudo-spherical aggregates of particles with average diameter of ca. 50–100 nm (Fig. 2B'). The XRD characterization reveals the presence of the main relevant signals due to magnetite crystal phase (Fig. 2B), whereas the signal width confirms the presence of smaller particles rather than the reference M0, probably due to the action by HA during the particle growth [31,32]. After performing the thermal treatment necessary for the recycling process, the XRD analysis of the resulting HPT sample revels the presence of the main relevant reflections at $2\theta = 24.2°$ (012), 33.3° (104), 35.7° (110), 41.0° (113), 49.6° (024), 54.2° (116), 57.8° (018), 62.6° (214) and 64.2° (300), which can be associated to the presence of the fully oxidized hematite crystal phase (card number 01–089-8104, ICDD, Fig. 2C), thus indicating the occurrence of the magnetite-to-hematite transition [33,34]. The consequence of this is a morphological evolution toward rounded condensed nanostructures with average diameter of ca. 100–220 nm (Fig. 2C'), thus indicating the occurrence of condensation phenomena involving the starting HM nanoparticles. Following the proposed recycling process, HPT nanoparticles are used as source of Fe(III) for the synthesis of newly hybrid RHM samples. As demonstrated by the morphological and structural characterization, RHM particles are almost identical with the HM ones, with pseudo-spherical aggregates of particles with average diameter of ca. 50–100 nm (Fig. 2D'), and presence of the main relevant signals due to magnetite crystal phase (Fig. 2D). No XRD signals due to the presence of HA are detected in the XRD pattern of both HM and RHM, probably because below the limit of detection of the instrument (for the sake of comparison the XRD pattern of bare HA is reported in the *Supporting Information*, SI, **Fig. S1**) [35].

Interestingly, the crystallite average size estimated by the Scherrer equation (Eq. (1)) applied to the main intense XRD signal at ca. 35.4°2θ (311) for the two hybrids magnetite is 11 nm for HM and 12 nm for RHM. For the sake of comparison, the crystallite average size calculated for the bare magnetite M0 is 13 nm. The XRD result testifies that the nanoparticles scanned with the SEM analysis are primarily made by aggregates of smaller crystallites, whose diameter is in the ca. 10–13 nm range.

Fig. 3 reports the thermal and physicochemical characterization of bare reference substrates (HA, and M0), process intermediates (HPT) and hybrid nanomaterials (HM and RHM) in terms of TGA measurements carried out under air (oxidizing) atmosphere (Fig. 3A), and FTIR spectroscopy (Fig. 3B), respectively.

The thermal degradation of HA shows two main weight losses, the first one at ca. 100 °C (corresponding to ca. 9 wt%) due to the evaporation of physically sorbed water molecules (moisture), followed by a broad weight loss in the 250 °C–800 °C temperature range due to the decomposition of the HA organic (both aliphatic and aromatic) fraction,

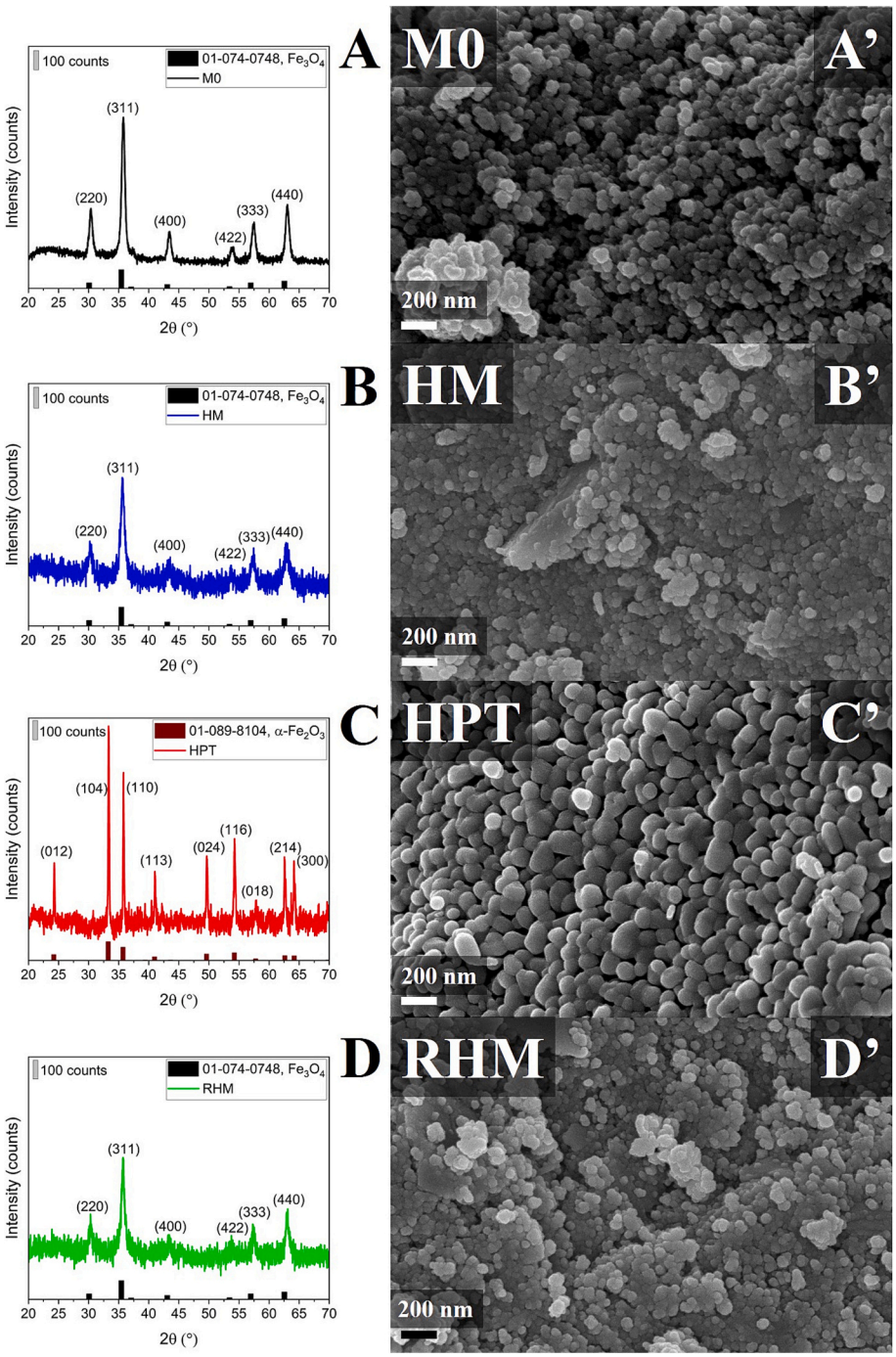

Fig. 2. XRD patterns (left), and SEM micrographs (right) of M0 (A, A'), HM (B, B'), HPT (C, C'), and RHM (D, D'). Legend: M0 (black), HM (blue), HPT (red), and RHM (green). XRD reference patterns: magnetite (01–074-0748, Fe_3O_4, black), and hematite (01–089-8104, α-Fe_2O_3, red).

leaving at 1000 °C a residue of ca. 37.6 wt% attributable to the presence of ashes and other inorganic residues (Fig. 3A) [20]. M0, instead, shows an almost negligible weight loss within the entire temperature range (corresponding to ca. 3 wt%), living at 1000 °C a reddish residue of ca. 97.1 wt%, thus indicating the absence of organic components, and the oxidation of the bare magnetite phase into the thermodynamically stable hematite phase. Regarding the hybrid magnetite-HA nanomaterials, the thermogram of the HM sample shows two main weight losses, the first one at ca. 100 °C (corresponding to ca. 3 wt%) due to the moisture evaporation, and a second one in the 250–400 °C temperature range (corresponding to ca. 15.6 wt%) primarily due to the decomposition of the organic fraction deriving from HA (but we cannot exclude the evolution of water coming from the iron oxide surface dehydration), leaving at 1000 °C a residue of ca. 79.6 wt% corresponding to the residual iron oxide. Analogously, the RHM sample shows a thermal profile similar to the HM sample, with two weight losses, the first one at ca. 100 °C (ca. 3 wt%), followed by a second one in the 250–400 °C temperature range (ca. 13.3 wt%), leaving at 1000 °C a residue of ca. 81.6 wt%. Lastly, the thermal analysis of the HPT sample (i.e., the intermediate hematite product sampled from the recycling process here proposed) confirms the goodness of the thermal treatment of the recycling process in Fig. 1 as a negligible weight loss (< 1 wt%) is registered within the entire temperature range (leaving a residue of ca. 99.8 wt%).

In order to confirm the chemical nature of the organic fraction in the

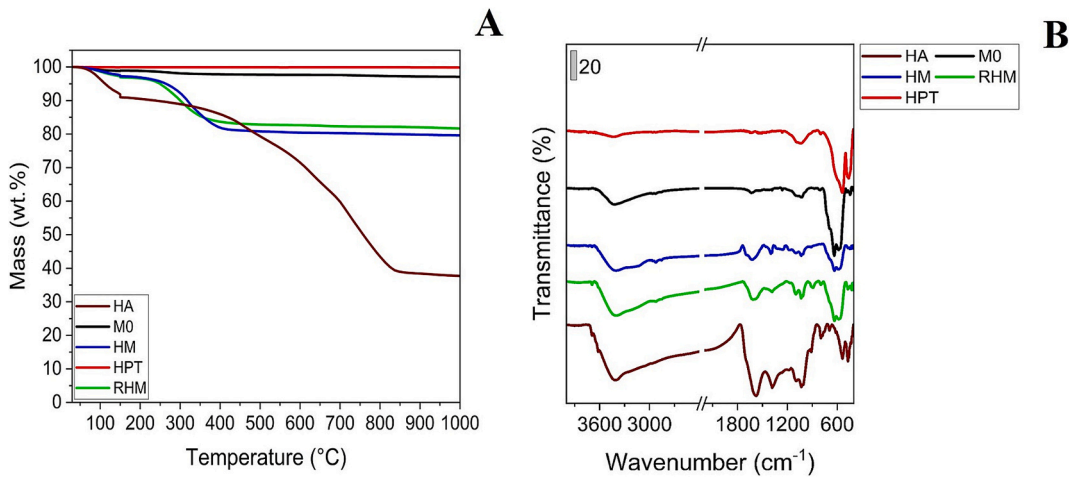

Fig. 3. TGA curves (A) and FTIR spectra in the 4000–400 cm^{-1} range (B) of HA, M0, HM, HPT, and RHM. Legend: HA (wine), M0 (black), HM (blue), HPT (red), and RHM (green).

hybrids, FTIR spectra of all samples are collected. In particular, the FTIR spectrum of bare HA shows a broad signal centered at ca. 3400 cm^{-1} attributable to the alcoholic and phenolic O—H stretching modes, followed by signals at ca. 1600 cm^{-1} due to carboxylate C═O and aliphatic C═C stretching modes, at ca. 1400 cm^{-1} due to O—H bending mode and phenolic C—O stretching mode, and at ca. 1100 cm^{-1} due to C—O bending mode of organic matter (e.g., polysaccharides) [4,36]. Bare magnetite M0, instead, shows the characteristic signals at ca. 640 cm^{-1} and ca. 580 cm^{-1} due to Fe—O stretching mode [4,37], coupled with weak signals at ca. 3400 cm^{-1} and ca. 1630 cm^{-1} attributable to the presence of traces of sorbed water. Interestingly, both HM and RHM show the main relevant IR signals attributable to the co-presence of the magnetite phase and the organic HA, thus confirming the previously discussed TGA outputs (Fig. 3A). For the sake of completeness, also the FTIR spectrum of HPT (i.e., the recycling process intermediate sampled after the thermal treatment) has been performed, registering the presence of signals at ca. 540 cm^{-1} and ca. 475 cm^{-1}, consistent with the presence of the hematite phase [37,38]. This last result confirms the absence of the characteristic IR signals of both magnetite and HA-derived organic fraction, in accordance to the outputs deriving from both the XRD (Fig. 2C) and TGA (Fig. 3A) characterizations.

Fig. 4 shows the room temperature TMS spectra of M0 (top), HM (middle) and RHM (bottom) samples. For all the samples, the data can be interpreted by the coexistence of two magnetically-split sextets ("A tetra" and "B octa") with an additional broad component in HM and RHM, as indicated with "unresolved doublet" in the Fig. 4's inset.

Table 1 summarizes the hyperfine parameters as obtained by fitting the data with the Vinda software package [39]: isomer shift (δ), quadrupole splitting (Δ), hyperfine magnetic field (B_{hf}), linewidth (Γ) and the relative area (%) of the detected components by assuming the same recoilless-free fraction equal to 1. The δ are given relative to α-Fe.

The hyperfine parameters of "A tetra" and "B octa" detected in M0 (Table 1) are compatible, respectively, with those expected for Fe^{3+} in the A-tetrahedral site, and $Fe^{2.5+}$ (i.e., equal number of Fe^{3+} and Fe^{2+} ions) in the B-octahedral site, of magnetite nanoparticles [40,41]. Slight differences are observed in the δ and B_{hf} values, which we interpret as it follows. In the case of "Fe^{3+}" (A tetra) contribution, we observe a higher δ when compared to the δ ca. 0.26 mm s^{-1} reported for bulk Fe_3O_4, while for the "$Fe^{2.5+}$" (B octa) contribution, we measure a marked reduction of δ than the expected δ ca. 0.67 mm s^{-1}. While the coexistence of the two sextets reflects that the chemical-structural nature of M0 is still that of magnetite in accordance with XRD (Fig. 2), from TMS we conclude that there is a large tendency for the Fe atoms to move from the Fe^{2+} to the Fe^{3+} charge state [40]. Same arguments apply for the HM and RHM samples (Table 1).

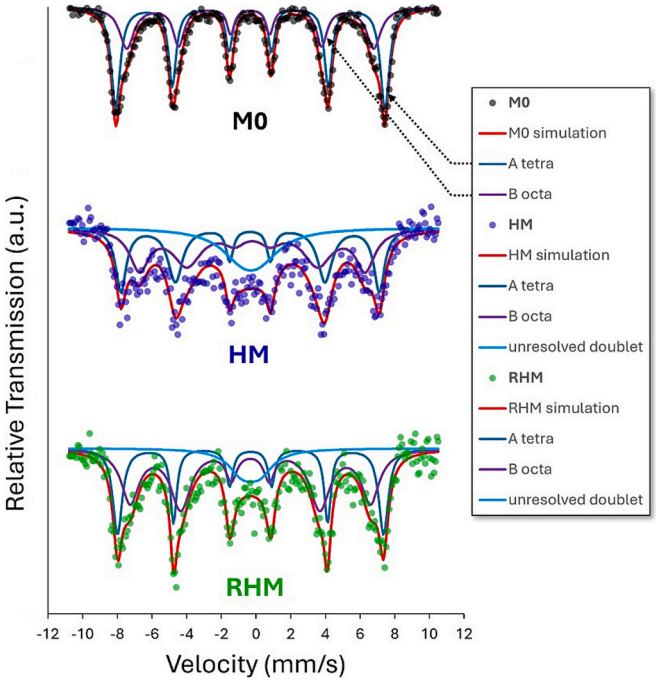

Fig. 4. TMS spectra obtained at RT for the M0 (top, black dots), HM (middle, violet dots), RHM (bottom, green dots) samples.

For all samples, the B_{hf} of both "A tetra" and "B octa" components are lower than in bulk Fe_3O_4, where we would expect respectively values around 49 T and 46 T [40,41]. This is most likely due to the increased number of Fe ions located at the surface of the nanoparticles, which also explains the tendency toward the Fe^{2+} to Fe^{3+} oxidation, even if a large fraction of Fe^{3+} still occupy the octahedral B-site (Table 1). Generally, a gradual broadening of spectral lines is observed when decreasing the particle diameter to few-nm, by finally approaching the superparamagnetic limit as reflected by the collapse of magnetically-split sextets into broad central lines [40,42–44] This may well be the origin for the emerging "unresolved doublet" component detected in HM and RHM, where in accordance with the crystallite average size estimated by the Scherrer equation (Fig. 2), smaller particles are observed when compared to M0. This is also in agreement with the overall superparamagnetic behavior detected by VSM (vide infra), where HM and RHM are characterized by null remanence and coercive field.

Table 1
Hyperfine parameters (isomer shift δ, quadrupole splitting Δ, hyperfine magnetic field B_{hf}, and average linewidth Γ) obtained from the fit of the TMS spectra of samples HM and RHM. The relative spectral area (%) is also indicated, by assuming an identical recoilless factor equal to 1.

	M0		HM			RHM		
	A tetra	*B octa*	*A tetra*	*B octa*	*"unres.doublet"*	*A tetra*	*B octa*	*"unres.doublet"*
δ (mm s^{-1})	0.326(2)	0.333(6)	0.34(1)	0.21(2)	–	0.31(1)	0.33(1)	–
Δ (mm s^{-1})	0	0	0	0	–	0	0	–
B_{hf} (T)	48.06(2)	44.08(2)	46.2(1)	40.3(2)	–	47.5(1)	42.9(1)	–
Γ (mm s^{-1})	0.54(2)	0.75(6)	0.7(1)	1.6(3)	–	0.5(1)	1.1(1)	–
%	60(1)	40(1)	36(1)	43(1)	21(1)	34(2)	53(2)	13(2)

In Johnson et al. [40] it has been shown that the transition from well-resolved magnetically-split sextets to broad superparamagnetic components, may occur in a very narrow particles' size change from 11.9 nm to 10.6 nm, which is surprisingly very close to the average diameters we estimate form XRD (see discussion about Scherrer analysis in Fig. 2).

Quite surprisingly, by judging the TMS data (Fig. 4 and Table 1), it emerges that RHM seems closer to M0 than HM. This demonstrates a very efficient resynthesizing process, which recovers the chemical, structural, and magnetic properties of Fe_3O_4, also as observed at the most atomic-scale.

Fig. 5 reports the magnetization curves measured by means of VSM of bare reference M0, and the two hybrid nanomaterials HM and RHM, whereas numerical parameters are summarized in Table 2. According to the experimental profile, all samples show superparamagnetic behavior [45]. Bare reference magnetite M0 shows magnetization saturation (M_s) value equal to ca. 74.4 emu g^{-1}, a very low intrinsic coercivity (H_c; ca. 3.2 Oe), and almost zero magnetic remanence (M_r; ca. 0.4 emu g^{-1}). Both hybrid nanomaterials show comparable M_s values (i.e., ca. 48.8 emu g^{-1} for HM, and ca. 44.1 emu g^{-1} for RHM), and negligible H_c and M_r values. Interestingly, the decrease of the M_s values for hybrid nanomaterials compared to neat magnetite follows the order M0> > HM ≈ RHM. This particular trend can be attributed to different factors, namely: (i) the possible different sizes of the magnetic domains forming the nanoparticles, (ii) the presence of organic species forming the hybrid systems (HM and RHM), and (iii) the occurrence of quenching phenomena involving the surface spin magnetic moments caused by an increased disorder of the organic binding ligands (in our case HA) as the particles decrease in size [4,46]. Furthermore, the M0> > HM ≈ RHM trend is confirmed even performing the mass normalization (data not shown for the sake of brevity).

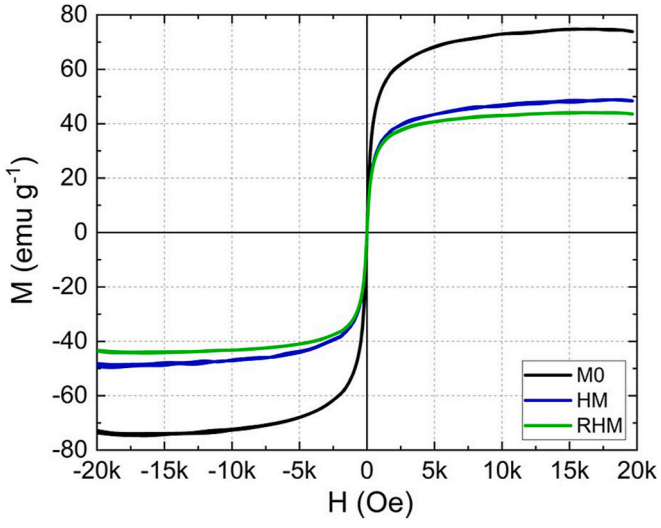

Fig. 5. Magnetization curves M vs. H of M0 (black), HM (blue), and RHM (green) samples.

Table 2
Magnetic properties of M0, HM, and RHM samples measured at RT.

Sample name	M_s (emu g^{-1})	M_r (emu g^{-1})	H_c (Oe)
M0	74.4	0.4	3.2
HM	48.8	0.0	0.0
RHM	44.1	0.0	0.0

3.2. Photocatalytic abatement of paracetamol in aqueous medium

Preliminary photocatalytic experiments are carried out to assess the performance of the two hybrid nanomaterials (HM and RHM) toward the abatement of contaminants investigating a photo-Fenton degradation route, selecting paracetamol (a non-steroidal anti-inflammatory drug) as target pollutant. The photostability of paracetamol under the experimental conditions is reported in the *Supporting Information* (**Fig. S2**), whereas the photocatalytic behavior of the different substrates (i.e., M0, HM and RHM) as a function of the (UV irradiation) time is reported in Fig. 6. For completeness, the variation of the experimental absorbance UV–Vis spectra in the 200–400 nm range relative to the paracetamol solution during the (photo)catalytic tests are reported in the *Supporting Information* (**Fig. S3**).

The photostability of the paracetamol aqueous solution has been preliminary assessed in homogeneous conditions under UV irradiation either in absence (i.e., UV) or presence of H_2O_2 (i.e., UV/H_2O_2). From the trend reported in **Fig. S2**, no significant degradation of paracetamol has been observed under UV irradiation (absence of photolysis). By introducing H_2O_2, at the experimental conditions selected (UV/H_2O_2)

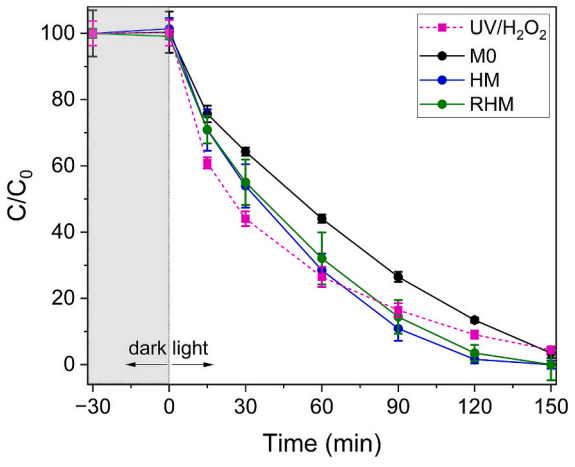

Fig. 6. Photocatalytic tests expressed as relative concentration of paracetamol as a function of the (irradiation) time in photo-Fenton conditions (UV/H_2O_2). Degradation of paracetamol in presence of only H_2O_2 (magenta squares, magenta dashed line), M0 (black circles, black solid line), HM (blue circles, blue solid line), and RHM (green circles, green solid line). Initial conditions: [paracetamol] 30 mg L^{-1}, [H_2O_2] 3.7 mM, [magnetite] 100 mg L^{-1}, UV irradiation. Tests are carried out at natural pH. The error bars represent the standard errors of duplicate experiments.

the paracetamol concentration decreases by ca. 84 % after 90 min, and by ca. 96 % after 150 min, according to analogous systems in the literature [22,47], the paracetamol degradation in presence of H_2O_2 under UV irradiation is mainly attributed to the photo-catalytical action of the hydroxyl radicals generated by H_2O_2 photolysis.

Regarding the magnetite-based nanomaterials object of the present study, tests are initially performed in the dark (the first 30 min) to reach the adsorption equilibrium, subsequently the UV light has been switched on, and H_2O_2 inoculated. As highlighted by the trends in Fig. 6, in all cases the adsorption effect is negligible. Regarding the photocatalytic tests, the addition of bare magnetite M0 in presence of both H_2O_2 and UV irradiation causes an initial delay of the paracetamol degradation compared to the tests performed in absence of M0 (i.e., after 90 min of irradiation the residual paracetamol is ca. 26.5 % in the case of M0, and ca. 16.4 % in the case of UV/H_2O_2), whereas after 150 min of irradiation there is an inversion point, with ca. 3.5 % of residual paracetamol in the case of M0 and ca. 4.4 % in the case of UV/H_2O_2. On the contrary, the addition of the two hybrid nanomaterials (HM and RHM) changes the paracetamol degradation profiles. In detail, both degradation profiles are almost superimposable between each other, thus confirming once again the comparable activity of the two hybrid nanomaterials, and consequently the efficacy of the recycling route here proposed. Interestingly, both hybrid systems promote the almost complete degradation of paracetamol after 120 min of UV irradiation, with residual paracetamol of ca. 1.6 % and ca. 3.5 % in the case of HM and RHM, respectively. Even if the obtained results are quite moderate compared to previous studies [4,13,21], they are at least comparable with the ones reported by Palma et al. [22]. Moreover, the performances of both hybrid systems HM and RHM are still better than in the case of simply UV/H_2O_2 (residual paracetamol ca. 9.0 % after 120 min of irradiation) and bare magnetite M0 (ca. 13.4 %).

Trying to find a rationale, all tests done so far have highlighted that these systems, although promising, still present several criticalities, one above all their strong dependence from the organic fraction (which favors the particles dispersion, and provides functionalities able to form photoactive complexes with iron) [22]. By making a consideration over the composition of the nanomaterials (and, in particular, the content of the organic shell), the amount of organic fraction in the hybrid systems here discussed (HM and RHM) can be estimated being ca. 13–16 wt% (by means of TGA characterization), thus analogous to the ones calculated by Palma et al. (i.e., below 15 wt%) [22], but remarkably lower than the more efficient systems reported by Franzoso et al. (i.e., 35 wt%) [4]. Furthermore, according to the literature, there are experimental evidences that the efficiency of these types of heterogeneous photo-Fenton oxidation mechanism in presence of magnetite and HA strongly depends on two different aspects: (i) a surfactant-like effects due to the presence of the HA organic shell which enhances the NPs dispersion, as well as (ii) the release/dissolution of both organic moieties and soluble iron species from the solid phase, thus making the catalytic process primarily homogeneous [48]. According to the literature, in heterogeneous catalytic processes Fe^{2+} ions initiate the Fenton-process following the classical Haber-Weiss mechanism involving the oxidation of Fe^{2+} to Fe^{3+} and the decomposition of H_2O_2 into reactive hydroxyl radicals [49,50]. However, this process is reversible, and Fe^{3+} can be regenerated into Fe^{2+} through reaction with either H_2O_2 (Fenton conditions) or light radiation (photo-Fenton conditions) [50,51]. In a recent study by Molamahmood et al. [52], it has been reported the catalytic action of different iron oxides and oxyhydroxides against the decomposition of H_2O_2, confirming that this process is a surface-related heterogeneous process.

However, independently from mechanistic conclusions (which are out from the scope of the present study, and deserve further investigations with dedicated experiments), the photocatalytic tests clearly demonstrate that the hybrid magnetite-HA system obtained after the recovery cycle here proposed (RHM) shows analogous performances as the hybrid magnetite-HA system obtained from direct synthesis (HM).

3.3. Relevance of the results

This study addresses the topic of the recycling of end-of-life hybrid magnetite-HA nanosystems once they have exhausted their photocatalytic action in the environmental remediation of contaminated wastewater. In recent years, the research based on the use of magnet-sensitive materials for the remediation of contaminated wastewater has been remarkably intensified. The reasons behind this are at least four, all related to each other. First, as already discussed in the introduction of the present study, almost half of the human population lives in countries that suffer from water scarcity, and the global supply of fresh water deriving from the continental rainfall is not enough to accomplish the global water demand, thus providing an efficient (and virtuous) recycling of water is becoming always more an important technological solution for a transition toward a more circular water management. Second, the easiest way to provide an efficient recycling of wastewater in a controlled way is to consider technologies integrable into water treatments plants, which are facilities already available nearby the most populated metropolis/cities and able to daily treat large volumes of contaminated water. Third, treating large volume of water containing traces of contaminants opens to new concerns, such as the increasing growth of persistent emerging contaminants, hardly removable by traditional processes. Finally, in view of a more sustainable development, magnetite-based heterogeneous photo-Fenton is surely among the most promising photocatalytic approaches for the removal of organic contaminants from aqueous environment as it merges the advantages of a clean technology based on the use of UV radiation (which in perspective can be further substituted with the cheapest solar radiation), and the use of environmental-friendly magnet-sensitive substrates, easy removable from the aqueous medium, by simply applying an external magnetic field.

However, to the best of the authors' knowledge, the use of such magnetite-based approach, even if promising, has not yet found industrial applications, as several technological and engineering issues are actually still open. Among the open problems, there is for sure the fate of the photocatalysts once they exhausted their activity against the organic emerging contaminants. In fact, the scientific literature already pointed out that the key mechanism for this type of process requires an important contribution due to homogeneous phase reactions involving the soluble iron release, with a consequent decrease of the catalytic efficient with the cycling [22].

The results of the present study explore the possibility of extending the life of these magnetic systems by fully recovering them, and converting the exhausted materials into useful matter exploitable for resynthesizing novel hybrid magnetite-HA nanoparticles showing comparable features as the starting systems. In order to provide some economic considerations on the produced products, it should be pointed out that the overall cost (simply in terms of raw materials, and normalizing the synthesis respect to 1 g of product) for HM corresponds to ca. 6.07 €/1 g, whereas in the case of RHM systems, it corresponds to ca. 5.97 €/1 g. If we consider also the further cost due to the thermal treatment performed in a muffle oven in the case of the RHM synthesis, the overall cost can rise to more than ca. 8 €. However, in this simplistic economic analysis, we need to consider also the disposal costs of HM, which will further rise their total cost.

For the sake of completeness, it is important to underline that the here proposed recycling process requires a thermal treatment (which, however, can be modulated depending on the characteristics of the selected organic component that should be removed), and an acid digestion, which are both not properly environmental-friendly routes. However, it should be point out that these approaches are mandatory for obtaining an acid solution containing Fe(III) ions, without traces of organic matter. Furthermore, both these approaches are simple technologies easily-integrable in ordinary processes and exploitable also in other side-processes (e.g., conveying hot fumes deriving from the thermal treatment into a heat exchanger can reduce the cost associated to

this step). Additionally, the possibility of separating the CO_2 produced during the calcination step before being release in the atmosphere with strategies for carbon capture utilization and storage (CCUS) is an interesting strategy that can further increase the potentiality of the proposed protocol [53,54].

Therefore, even if the catalytic tests here proposed show some limitations (further studies are still necessary to optimize the testing conditions), the preliminary results here resumed clearly show that the use of magnetite-based nanomaterials in photocatalytic remediation processes of contaminated wastewater remains a very appealing technological solution, and it is possible to fully recycle end-of-life hybrid magnetite-HA nanosystems for obtaining novel systems suitable for the designed purpose.

4. Conclusions

The present manuscript reports a case study showing a recycling process involving hybrid magnetite-HA nanoparticles (HM in the text) to obtain newly synthesized hybrid nanoparticles (RHM in the text) with the same features of the starting nanosystems. In detail, HM nanoparticles are synthesized following a co-precipitation route, whereas RHM nanoparticles are obtain following a two-step process, namely: (i) calcination under air (oxidizing) atmosphere of the HM particles to both burn the organic fraction, and convert the inorganic fraction into the fully oxidized hematite, and (ii) acid digestion of hematite to obtain an acid Fe(III) aqueous solution. Subsequently, after neutralization, the RHM nanoparticles are resynthesized following a properly modified co-precipitation route analogous to the previous one.

Morphological, structural, physicochemical and magnetic variations between HM and RHM are monitored by SEM, XRD, TGA, FTIR and transmission Mössbauer spectroscopies, and VSM. Results evidenced that both systems show analogous features between each other. Finally, preliminary photocatalytic experiments are carried out to assess the performance of the two hybrid nanomaterials (HM and RHM) toward the abatement of paracetamol in a model wastewater, investigating a photo-Fenton degradation route. Experimental results point out: (i) the absence of adsorption phenomena (in the dark), (ii) both degradation profiles are almost superimposable between each other, (iii) both hybrid systems promote the almost complete degradation of paracetamol after 120 min of UV irradiation, with residual paracetamol of ca. 1.6 % and 3.5 % in the case of HM and RHM, respectively.

In conclusions, the experimental data reported in this study indicate that the recycling process here proposed is an effective route for the fully recycling of the hybrid magnetite-HA nanosystems, and that the photocatalytic tests performed, although preliminary, encourage on the possibility of using these magnetic hybrids for the abatement of recalcitrant contaminants from aqueous media in a clean way.

Author statement

We confirm that the manuscript has been read and approved by all named authors and that there are no other individuals who meet the criteria for authorship but have not been listed. Additionally, we affirm that the article has not been previously published in other journals and is free from plagiarism or any potential copyright disputes.

CRediT authorship contribution statement

Gabriele Bona: Writing – review & editing, Investigation, Formal analysis. **Lorenzo Viganò:** Writing – review & editing, Investigation, Formal analysis. **Matteo Cantoni:** Writing – review & editing, Writing – original draft, Supervision, Resources, Investigation, Formal analysis. **Roberto Mantovan:** Writing – review & editing, Writing – original draft, Supervision, Resources, Investigation, Data curation. **Barbara Di Credico:** Writing – review & editing, Resources, Investigation. **Silvia Mostoni:** Writing – review & editing, Investigation. **Roberto Scotti:** Writing – review & editing, Supervision, Resources, Investigation. **Roberto Nisticò:** Writing – review & editing, Writing – original draft, Supervision, Resources, Investigation, Formal analysis, Conceptualization.

Declaration of competing interest

The authors declare that they have no known competing financial interests or personal relationships that could have appeared to influence the work reported in this paper.

Data availability

Data will be made available on request.

Acknowledgements

The idea behind this study came in response to interesting questions raised by colleagues during the oral presentations R.N. gave at the Friday Materials Science Colloquia of the University of Milano-Bicocca (Milano, Italy) and at the XLVIII Italian Conference of Inorganic Chemistry (Pisa, Italy). The magnetic characterization was performed at Polifab, the micro and nanofabrication facility of Politecnico di Milano. Authors would like to acknowledge Dr. Paolo Gentile and Dr. Fabrizio Vergani (University of Milano-Bicocca, Italy) for the technical support during the SEM analysis. This work received financial support from MUR (Italy) and the European Union – Next Generation EU, Mission 4, Component 1, CUP (H53D23004490001) through the PRIN Project MAPEC (N. 2022599NR3), and CUP (H53D23008000001) through the PRIN Project PERFECT (N. P2022TK9B9). University of Milano-Bicocca is gratefully acknowledged for funding project Premio Giovani Talenti 2022.

Appendix A. Supplementary data

Supplementary data to this article can be found online at https://doi.org/10.1016/j.susmat.2025.e01275.

References

[1] C. He, Z. Liu, J. Wu, X. Pan, Z. Fang, J. Li, B.A. Bryan, Future global urban water scarcity and potential solutions, Nat. Commun. 12 (2021) 4667, https://doi.org/10.1038/s41467-021-25026-3.
[2] M. van Vliet, M. Florke, Y. Wada, Quality matters for water scarcity, Nat. Geosci. 10 (2017) 800–802, https://doi.org/10.1038/ngeo3047.
[3] A. Boretti, L. Rosa, Reassessing the projections of the world water development report, npj Clean Water 2 (2019) 15, https://doi.org/10.1038/s41545-019-0039-9.
[4] F. Franzoso, R. Nisticò, F. Cesano, I. Corazzari, F. Turci, D. Scarano, A. Bianco Prevot, G. Magnacca, L. Carlos, D.O. Martire, Biowaste-derived substances as a tool for obtaining magnet-sensitive materials for environmental applications in wastewater treatments, Chem. Eng. J. 310 (2017) 307–316, https://doi.org/10.1016/j.cej.2016.10.120.
[5] S. Zahmatkesh, M. Hajiaghaei-Keshteli, A. Bokhari, S. Sundaramurthy, B. Panneerselvam, Y. Rezakhani, Wastewater treatment with nanomaterials for the future: a state-of-the-art review, Environ. Res. 216 (2023) 114652, https://doi.org/10.1016/j.envres.2022.114652.
[6] S.F. Ahmed, M. Mofijur, B. Ahmed, T. Mehnaz, F. Mehejabin, D. Maliat, A. T. Hoang, G.M. Shafiullah, Nanomaterials as a sustainable choice for treating wastewater, Environ. Res. 214 (2022) 113807, https://doi.org/10.1016/j.envres.2022.113807.
[7] E. Pargoletti, S. Mostoni, G. Rassu, V. Pifferi, D. Meroni, L. Falciola, E. Davoli, M. Marelli, G. Cappelletti, Zn- vs Bi-based oxides for o-toluidine photocatalytic treatment under solar light, Environ. Sci. Pollut. Res. 24 (2017) 8287–8296, https://doi.org/10.1007/s11356-017-8430-x.
[8] S. Huang, L. Gu, N. Zhu, K. Feng, H. Yuan, Z. Lou, Y. Li, A. Shan, Heavy metal recovery from electroplating wastewater by synthesis of mixed-Fe_3O_4@SiO_2/metal oxide magnetite photocatalysts, Green Chem. 16 (2014) 2696–2705, https://doi.org/10.1039/C3GC42496K.
[9] A. de Oliveira Jorgetto, A. Milbrat, J.F. Schneider, G. Giammaria, M.J. Saeki, T. M. Ribeiro Gianeti, G.P. Pereira Lima, V. de Albuquerque Pedrosa, G. Mul, G. Rocha de Castro, Magnetically-extractable hybrid of magnetite, mesoporous silica and titania for the photo-degradation of organic compounds in water, Appl. Surf. Sci. 457 (2018) 121–133, https://doi.org/10.1016/j.apsusc.2018.06.218.

[10] N. Ferroudj, J. Nzimoto, A. Davidson, D. Talbot, E. Briot, V. Dupuis, A. Bee, M. S. Medjram, S. Abramson, Maghemite nanoparticles and maghemite/silica nanocomposite microspheres as magnetic Fenton catalysts for the removal of water pollutants, Appl. Catal. B Environ. 136-137 (2013) 9–18, https://doi.org/10.1016/j.apcatb.2013.01.046.
[11] J.C.S. Terra, A. Desgranges, C. Monnereau, E.H. Sanchez, J.A. De Toro, Z. Amara, A. Moores, Photocatalysis meets magnetism: designing magnetically recoverable supports for visible-light photocatalysis, ACS Appl. Mater. Interfaces 12 (2020) 24895–24904, https://doi.org/10.1021/acsami.0c06126.
[12] A. Bianco Prevot, F. Baino, D. Fabbri, F. Franzoso, G. Magnacca, R. Nisticò, A. Arques, Urban biowaste-derived sensitizing materials or caffeine photodegradation, Environ. Sci. Pollut. Res. 24 (2017) 12599–12607, https://doi.org/10.1007/s11356-016-7763-1.
[13] R. Nisticò, A. Bianco Prevot, G. Magnacca, L. Canone, S. Garcia-Ballesteros, A. Arques, Sustainable magnetic materials (from chitosan and municipal biowaste) for the removal of Diclofenac from water, Nanomaterials 9 (2019) 1091, https://doi.org/10.3390/nano9081091.
[14] R. Nisticò, Magnetic materials and water treatments for a sustainable future, Res. Chem. Intermed. 43 (2017) 6911–6949, https://doi.org/10.1007/s11164-017-3029-x.
[15] S. Giannakis, S. Liu, A. Carratalà, S. Rtimi, M.T. Amiri, M. Bensimon, C. Pulgarin, Iron oxide-mediated semiconductor photocatalysis vs. heterogeneous photo-Fenton treatment of viruses in wastewater. Impact of the oxide particle size, J. Hazard. Mater. 339 (2017) 223–231, https://doi.org/10.1016/j.jhazmat.2017.06.037.
[16] C. Ruales-Lonfat, J.F. Barona, A. Sienkiewicz, M. Bensimon, J. Velez-Colmenares, N. Benitez, C. Pulgarin, Iron oxides semiconductors are efficients for solar water disinfection: a comparison with photo-Fenton processes at neutral pH, Appl. Catal. B Environ. 166-167 (2015) 497–508, https://doi.org/10.1016/j.apcatb.2014.12.007.
[17] J. He, X. Yang, B. Men, D. Wang, Interfacial mechanisms of heterogeneous Fenton reactions catalyzed by iron-based materials: a review, J. Environ. Sci. 39 (2016) 97–109, https://doi.org/10.1016/j.jes.2015.12.003.
[18] P. Avetta, F. Bella, A. Bianco Prevot, E. Laurenti, E. Montoneri, A. Arques, L. Carlos, Waste cleaning waste: Photodegradation of monochlorophenols in the presence of waste-derived photosensitizer, ACS Sustainable Chem. Eng. 1 (2013) 1545–1550, https://doi.org/10.1021/sc400294z.
[19] D. Palma, A. Bianco Prevot, L. Celi, M. Martin, D. Fabbri, G. Magnacca, M. R. Chierotti, R. Nisticò, Isolation, characterization, and environmental application of bio-based materials as auxiliaries in photocatalytic processes, Catalysts 8 (2018) 197, https://doi.org/10.3390/catal8050197.
[20] E. Montoneri, R. Nisticò, M. Francavilla, Demineralisation of municipal biowaste hydrolysates, ChemistrySelect 4 (2019) 7551–7554, https://doi.org/10.1002/slct.201900369.
[21] V. Polliotto, F.R. Pomilla, V. Maurino, G. Marcì, A. Bianco Prevot, R. Nisticò, G. Magnacca, M.C. Paganini, L. Ponce Robles, L. Perez, S. Malato, Different approaches for the solar photocatalytic removal of micro-contaminants from aqueous environment: Titania vs. hybrid magnetic iron oxides, Cat. Today 328 (2019) 164–171, https://doi.org/10.1016/j.cattod.2019.01.044.
[22] D. Palma, A. Bianco Prevot, M. Brigante, D. Fabbri, G. Magnacca, C. Richard, G. Mailhot, R. Nisticò, New insights on the photodegradation of caffeine in the presence of bio-based substances-magnetic iron oxide hybrid nanomaterials, Materials 11 (2018) 1084, https://doi.org/10.3390/ma11071084.
[23] A. Nyabadza, M. Makhesana, A. Plouze, A. Kumar, I. Ramirez, S. Krishnamurthy, M. Vazquez, D. Brabazon, Advanced nanomaterials and dendrimers in water treatment and the recycling of nanomaterials: a review, J. Environ. Chem. Eng. 12 (2024) 112643, https://doi.org/10.1016/j.jece.2024.112643.
[24] R.K. Gautam, I. Tiwari, Humic acid functionalized magnetic nanomaterials for remediation of dye wastewater under ultrasonication: application in real water samples, recycling and reuse of nanosorbents, Chemosphere 245 (2020) 125553, https://doi.org/10.1016/j.chemosphere.2019.125553.
[25] R. Kumar, R. Sakthivel, R. Behura, B.K. Mishra, D. Das, Synthesis of magnetite nanoparticles from mineral waste, J. Alloys Compd. 645 (2015) 398–404, https://doi.org/10.1016/j.jallcom.2015.05.089.
[26] M.E. Peralta, R. Nisticò, F. Franzoso, G. Magnacca, L. Fernandez, M.E. Parolo, E. G. Leon, L. Carlos, Highly efficient removal of heavy metals from waters by magnetic chitosan-based composite, Adsorption 25 (2019) 1337–1347, https://doi.org/10.1007/s10450-019-00096-4.
[27] R. Nisticò, A synthetic guide toward the tailored production of magnetic iron oxide nanoparticles, Bol. Soc. Esp. Ceram. V. 60 (2021) 29–40, https://doi.org/10.1016/j.bsecv.2020.01.011.
[28] M.A. Wells, R.J. Gilkes, R.W. Fitzpatrick, Properties and acid dissolution of metal-substituted hematites, Clay Clay Miner. 49 (2001) 60–72, https://doi.org/10.1346/CCMN.2001.0490105.
[29] M. Parolini, Toxicity of the non-steroidal anti-inflammatory drugs (NSAIDs) acetylsalicylic acid, paracetamol, diclofenac, ibuprofen and naproxen towards freshwater invertebrates: a review, Sci. Total Environ. 740 (2020) 140043, https://doi.org/10.1016/j.scitotenv.2020.140043.
[30] M. D'Arienzo, J. Carbajo, A. Bahamonde, M. Crippa, S. Polizzi, R. Scotti, L. Wahba, F. Morazzoni, Photogenerated defects in shape-controlled TiO_2 anatase nanocrystals: a probe to evaluate the role of crystal facets in photocatalytic processes, J. Am. Chem. Soc. 133 (2011) 17652–17661, https://doi.org/10.1021/ja204838s.
[31] R. Nisticò, F. Franzoso, F. Cesano, D. Scarano, G. Magnacca, M.E. Parolo, L. Carlos, Chitosan-derived iron oxide systems for magnetically guided and efficient water purification processes from polycyclic aromatic hydrocarbons, ACS Sustain. Chem. Eng. 5 (2017) 793–801, https://doi.org/10.1021/acssuschemeng.6b02126.
[32] V. Venezia, G. Pota, B. Silvestri, G. Vitiello, P. Di Donato, G. Landi, V. Mollo, M. Verrillo, S. Cangemi, A. Piccolo, G. Luciani, A study on structural evolution of hybrid humic acids-SiO_2 nanostructures in pure water: effects on physico-chemical and functional properties, Chemosphere 287 (2022) 131985, https://doi.org/10.1016/j.chemosphere.2021.131985.
[33] G. Bona, G. Bragaggia, M. Cantoni, B. Di Credico, S. Mostoni, G. Capitani, R. Scotti, S. Gross, R. Nisticò, Polyethylene glycol-assisted hydro-solvothermal growth of anisotropic magnetic iron oxides: the role of mixed environment conditions, Colloids Surf. A Physicochem. Eng. Asp. 702 (2024) 135117, https://doi.org/10.1016/j.colsurfa.2024.135117.
[34] F. Cesano, G. Fenoglio, L. Carlos, R. Nisticò, One-step synthesis of magnetic chitosan polymer composite films, Appl. Surf. Sci. 345 (2015) 175–181, https://doi.org/10.1016/j.apsusc.2015.03.154.
[35] C. He, J. Qu, Z. Yu, D. Chen, T. Su, L. He, Z. Zhao, C. Zhou, P. Hong, Y. Li, S. Sun, C. Li, Preparation of micro-nano material composed of oyster shell/Fe_3O_4 nanoparticles/humic acid and its application in selective removal of Hg(II), Nanomaterials 8 (2019) 953, https://doi.org/10.3390/nano9070953.
[36] R. Baigorri, M. Fuentes, G. Gonzalez-Gaitano, J.M. Garcia-Mina, G. Almendros, F. J. Gonzalez-Villa, Complementary multianalytical approach to study the distinctive structural features of the main humic fractions in solution: Gray humic acid, brown humic acid, and fulvic acid, J. Agric. Food Chem. 57 (2009) 3266–3272, https://doi.org/10.1021/jf8035353.
[37] Y.-S. Li, J.S. Church, A.L. Woodhead, Infrared and Raman spectroscopic studies on iron oxide magnetic nano-particles and their surface modifications, J. Magn. Magn. Mater. 324 (2012) 1543–1550, https://doi.org/10.1016/j.jmmm.2011.11.065.
[38] S.M. Rodulfo-Baechler, S.L. Gonzalez-Cortes, J. Orozco, V. Sagredo, B. Fontal, A. J. Mora, G. Delgado, Characterization of modified iron catalysts by X-ray diffraction, infrared spectroscopy, magnetic susceptibility and thermogravimetric analysis, Mater. Lett. 58 (2004) 2447–2450, https://doi.org/10.1016/j.matlet.2004.02.032.
[39] H.P. Gunnlaughsson, Spreadsheet based analysis of Mössbauer spectra, Hyperfine Interact. 237 (2016) 79, https://doi.org/10.1007/s10751-016-1271-z.
[40] C.E. Johnson, J.A. Johnson, H.Y. Hah, M. Cole, S. Gray, V. Kolesnichenko, P. Kucheryavy, G. Goloverda, Mössbauer studies of stoichiometry of Fe_3O_4: characterization of nanoparticles for biomedical applications, Hyperfine Interact. 237 (2016) 27, https://doi.org/10.1007/s10751-016-1277-6.
[41] M.A. Shipilin, I.N. Zakharova, A.M. Shipilin, V.I. Bachurin, Mössbauer studies of magnetite nanoparticles, J. Surf. Investig. 8 (2014) 557–561, https://doi.org/10.1134/S1027451014030343.
[42] J. Fock, M. Fougt Hansen, C. Frandsen, S. Morup, On the interpretation of Mössbauer spectra of magnetic nanoparticles, J. Magn. Magn. Mater. 445 (2018) 11–21, https://doi.org/10.1016/j.jmmm.2017.08.070.
[43] A. Joos, C. Rumenapp, F.E. Wagner, B. Gleich, Characterisation of iron oxide nanoparticles by Mössbauer spectroscopy at ambient temperature, J. Magn. Magn. Mater. 399 (2016) 123–129, https://doi.org/10.1016/j.jmmm.2015.09.060.
[44] H.Y. Hah, S. Gray, C.E. Johnson, J.A. Johnson, V. Kolesnichenko, P. Kucheryavy, G. Goloverda, Mössbauer spectroscopy of superparamagnetic Fe_3O_4 nanoparticles, J. Magn. Magn. Mater. 539 (2021) 168382, https://doi.org/10.1016/j.jmmm.2021.168382.
[45] R. Nisticò, F. Cesano, F. Garello, Magnetic materials and systems: domain structure visualization and other characterization techniques for the application in the materials science and biomedicine, Inorganics 8 (2020) 6, https://doi.org/10.3390/inorganics8010006.
[46] E.D. Smolensky, H.-Y.E. Park, Y. Zhou, G.A. Rolla, M. Marjanska, M. Botta, V. C. Pierre, Scaling laws at the nanosize: the effect of particle size and shape on the magnetism and relaxivity of iron oxide nanoparticle contrast agents, J. Mater. Chem. B 1 (2013) 2818–2828, https://doi.org/10.1039/C3TB00369H.
[47] D. Vogna, R. Marotta, A. Napolitano, M. d'Ischia, Advanced oxidation chemistry of paracetamol. UV/H_2O_2-induced hydroxylation/degradation pathways and ^{15}N-aided inventory of nitrogenous breakdown products, J. Org. Chem. 67 (2002) 6143–6151, https://doi.org/10.1021/jo025604v.
[48] M. Munoz, Z.M. de Pedro, J.A. Casas, J.J. Rodriguez, Preparation of magnetite-based catalysts and their application in heterogeneous Fenton oxidation – a review, Appl. Catal. B Environ. 176-177 (2015) 249–265, https://doi.org/10.1016/j.apcatb.2015.04.003.
[49] M. Minella, G. Marchetti, E. De Laurentiis, M. Malandrino, V. Maurino, C. Minero, D. Vione, K. Hanna, Photo-Fenton oxidation of phenol with magnetite as iron source, Appl. Catal. B Environ. 154-155 (2014) 102–109, https://doi.org/10.1016/j.apcatb.2014.02.006.
[50] Y. Zhu, Q. Xie, F. Deng, Z. Ni, Q. Lin, L. Cheng, X. Chen, R. Qiu, R. Zhu, The differences in heterogeneous Fenton catalytic performance and mechanism of various iron minerals and their influencing factors: a review, Sep. Purif. Technol. 325 (2023) 124702, https://doi.org/10.1016/j.seppur.2023.124702.
[51] S.A. Walling, W. Um, C.L. Corkhill, N.C. Hyatt, Fenton and Fenton-like wet oxidation for degradation and destruction of organic radioactive wastes, npj Mater. Degrad. 5 (2021) 50, https://doi.org/10.1038/s41529-021-00192-3.
[52] H.V. Molamahmood, W. Geng, Y. Wei, J. Miao, S. Yu, A. Shahi, C. Chen, M. Long, Catalyzed H_2O_2 decomposition over iron oxides and oxyhydroxides: insights from oxygen production and organic degradation, Chemosphere 291 (2022) 133037, https://doi.org/10.1016/j.chemosphere.2021.133037.
[53] A. Bang, D. Moreno, H. Lund, S. Nielsen, Regional CCUS strategies in the context of a fully decarbonized society, J. Clean. Prod. 477 (2024) 143882, https://doi.org/10.1016/j.jclepro.2024.143882.
[54] L. Miao, L. Feng, Y. Ma, Comprehensive evaluation of CCUS technology: a case study of China's first million-tonne CCUS-EOR project, Environ. Impact Assess. Rev. 110 (2025) 107684, https://doi.org/10.1016/j.eiar.2024.107684.